AGU PUBLICATIONS

Geophysical Research Letters

RESEARCH LETTER
10.1002/2016GL072443

Special Section:
Early Results: Juno at Jupiter

The first close-up images of Jupiter's polar regions: Results from the Juno mission JunoCam instrument

Glenn S. Orton[1], Candice Hansen[2], Michael Caplinger[3], Michael Ravine[3], Sushil Atreya[4], Andrew P. Ingersoll[5], Elsa Jensen[3], Thomas Momary[1], Leslie Lipkaman[3], Daniel Krysak[3], Robert Zimdar[3], and Scott Bolton[6]

[1]Jet Propulsion Laboratory, California Institute of Technology, Pasadena, California, USA, [2]Planetary Science Institute, Tucson, Arizona, USA, [3]Malin Space Science Systems, San Diego, California, USA, [4]Planetary Science Laboratory, University of Michigan, Ann Arbor, Michigan, USA, [5]Division of Geological and Planetary Sciences, California Institute of Technology, Pasadena, California, USA, [6]Southwest Research Institute, San Antonio, Texas, USA

Abstract During Juno's first perijove encounter, the JunoCam instrument acquired the first images of Jupiter's polar regions at 50–70 km spatial scale at low emission angles. Poleward of 64–68° planetocentric latitude, where Jupiter's east-west banded structure breaks down, several types of discrete features appear on a darker background. Cyclonic oval features are clustered near both poles. Other oval-shaped features are also present, ranging in size from 2000 km down to JunoCam's resolution limits. The largest and brightest features often have chaotic shapes. Two narrow linear features in the north, associated with an overlying haze feature, traverse tens of degrees of longitude. JunoCam also detected an optically thin cloud or haze layer past the northern nightside terminator estimated to be 58 ± 21 km (approximately three scale heights) above the main cloud deck. JunoCam will acquire polar images on every perijove, allowing us to track the state and evolution of longer-lived features.

Key Points:
- The JunoCam instrument obtained the first close-up images of Jupiter's polar regions with spatial scales of 50–70 km
- The color and morphology of features in polar regions are very different from lower latitudes and are unlike Saturn's polar regions
- The altitude of a haze layer above the main cloud deck in Jupiter's atmosphere was measured using JunoCam's view of the terminator

Supporting Information:
- Supporting Information S1

Correspondence to:
G. S. Orton,
glenn.orton@jpl.nasa.gov

Citation:
Orton, G. S., et al. (2017), The first close-up images of Jupiter's polar regions: Results from the Juno mission JunoCam instrument, *Geophys. Res. Lett.*, *44*, doi:10.1002/2016GL072443.

Received 23 DEC 2016
Accepted 5 MAR 2017

1. Introduction

JunoCam, the visible imager on the Juno spacecraft, was conceived as a vehicle for public participation in the Juno mission. The JunoCam investigation relies on ground-based telescope data from amateur astronomers for planning and prioritization of targets to be imaged. The JunoCam images are processed by citizen scientists. JunoCam also has an important science objective—to image the poles of Jupiter from a perspective not achieved by other missions and unavailable to Earth-based telescopes. Here we report on the first of those measurements made during Juno's close approach to Jupiter following its first orbit, known as Perijove 1, usually shortened to "PJ1." Juno is in an elliptical polar orbit around Jupiter. The spacecraft is directly over the north pole ~1 h before perijove and over the south pole ~1 h after perijove. This vantage point is a unique attribute of this mission, and the camera was designed to take advantage of it.

2. The JunoCam Instrument

JunoCam is a pushframe visible camera designed to take advantage of being located on a spinning spacecraft by using time-delayed integration (TDI) to build up signal. In one rotation, it acquires an image through broadband red, green, and blue filters mounted directly on the charge-coupled device. On a separate rotation, typically 30 s later, it acquires a narrowband image in the 889 nm methane absorption band. The 58° wide field of view, 1600 pixels across, captures the entire polar region in one image, with the other dimension supplied by the spacecraft rotation. The detailed description of the JunoCam instrument, including its construction, filter band passes, and operation is described by *Hansen et al*. [2014].

3. Description of the Polar Data

The JunoCam images during PJ1 were planned as a series of tests of the instrument parameters and performance in the Jovian environment. In this report, we discuss a subset of the 23 images obtained within a 2 h time interval centered on closest approach. The full set included tests to establish optimal TDI, attempts at stereographic pair observations, comparisons of results using various compression ratios, searches for lightning, and searches for visible aurora. These observations were preceded and followed by images acquired from greater distances to Jupiter, nicknamed as "marble movies" because of their high cadence

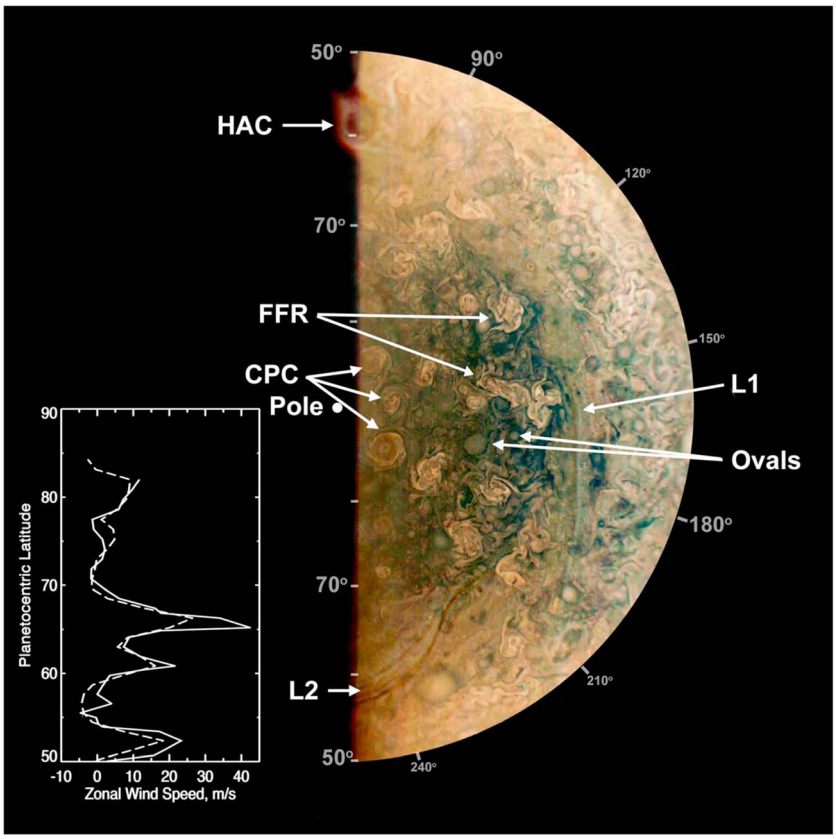

Figure 1. Polar projection of an RGB composite image of Jupiter's north polar region taken by JunoCam on 27 August 2016, at 11:59 from a distance of 73,009 km above Jupiter's cloud deck. This image resolves features down to 50 km in size. We identify the original image file name "JNCE_2016240_00C06160_V01" as simply image "6160," a simplification we use for other images discussed in this report. Compensation of solar illumination for the high-altitude cloud (labeled HAC) was done by adding the average daylight radiance to all positions in Jupiter's nightside then setting to 0 all that were equal only to the average. The following other features are labeled: circumpolar cyclones (CPC), folded filamentary regions (FFR), examples of ovals, and linear features (L1 and L2). The position of the north pole is in the nightside because of Jupiter's small but nonzero obliquity. The irregular low-latitude edges of the map result from edges of the frame of the original image or the presence of image saturation, which was removed from the map. Latitudes are shown on a planetocentric scale, and longitudes indicate System III values. The mean zonal wind speed profiles shown in the inserts in this figure and Figure 2 are derived from *Porco et al.* [2003] (dashed line) and *Barrado-Izagirre et al.* [2008] (solid line).

and characteristic spatial resolutions that are usually much lower than obtainable from very small ground-based telescopes. Figures 1 and 2 provide an overview of polar features in the north and south polar regions, respectively, that we discuss in more detail in the next section. These images have been processed to remove camera distortions and stretched to make subtle features more visible. We also corrected for the variation of solar illumination across the disk in each filter empirically by creating a lookup table formed from the global mean dependence of radiance as a function of incident solar angle in each filter. We then used that global variation to adjust the radiance of each pixel to a value at a common emission angle.

4. Results

4.1. Breakdown of Zonal Banding

Consistent with earlier imaging studies of Jupiter's polar regions by Pioneer 11 [see *Gehrels*, 1976] and Cassini [see *Porco et al.*, 2003; *Li et al.*, 2004; *Barrado-Izagirre et al.*, 2008], we note a dramatic change in the organization of the atmosphere poleward of 68°N latitude and 64°S latitude. (Note that we use planetocentric latitudes consistently throughout this report.) The strong east-west banded organization of lower latitudes breaks down, immediately poleward of a ~40 m/s prograde jet [*Porco et al.*, 2003; *Barrado-Izagirre et al.*,

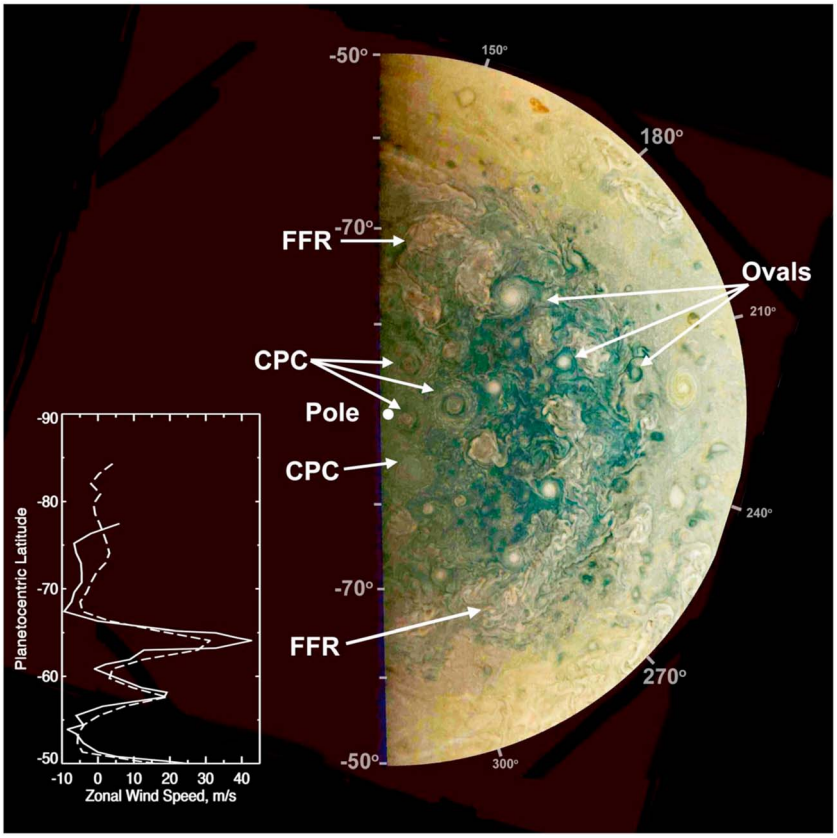

Figure 2. Polar projection of an RGB composite image of Jupiter's south polar region taken by JunoCam on 27 August 2016, at 13:56 UT from a distance of 95,096 km from the cloud deck, designated as image 6186. This image resolves features down to 70 km in size. The same processing was done to this projection as to the one in Figure 1. The same nomenclature is used as in Figure 1. Ovals indicate a variety of examples of different oval-shaped features. Both this figure and Figure 1 were based on decompanded (converted from 8 bits to 12 bits, based on the lookup table documented in NASA's Planetary Data System, Imaging Node) and geometrically calibrated versions of the original images provided by Gerald Eichstädt.

2008], as illustrated by the inserts in Figures 1 and 2, and a plethora of discrete features are present, ostensibly randomly distributed. This change in local morphology is consistent with the location of a dramatic decrease of zonal wind velocities at poleward latitudes. The overall appearance of the polar regions is one of a dark-colored background with a variety of discrete features, most of which are brighter. The discrete features are also generally brighter in methane band images (see supporting information), implying that they are distributed higher in altitude than the darker-colored background. The boundaries of the polar regions meander, which has been described as the possible manifestation of a Rossby wave [*Li et al*., 2004; *Barrado-Izagirre et al*., 2008]. However, there is no sign of a clearly defined hexagon or any other polygonal feature in either hemisphere, unlike the atmosphere of Saturn [*Godfrey*, 1988]. In this report, we will identify these regions as the north polar region (NPR) and the south polar region (SPR), corresponding to classical nomenclature [*Rogers*, 1995], although those definitions formally include regions poleward of 53°N and 49°S, respectively.

4.2. Circumpolar Cyclones

One of the most intriguing of the discrete polar features are tight clusters of circular-storm features close to both poles, which were undetected in previous observations because the viewing geometry was too oblique. In the north, three tightly packed storms can be seen centered at 83°–84°N latitude, approximately 2400–2800 km across, with a fourth partially visible (Figure 1, labeled "CPC"). The longitudinal spacing determined from this image is consistent with the presence of four other such features around the north pole, for a total of eight, assuming equal spacing in a complete circle. In the south, three such features are also seen, centered at 85°S–86°S and approximately 1700–2200 km across. Their longitudinal spacing implies a total

of five or six around the south pole, with a similar set of assumptions. One additional feature appears close to the pole at 88.5°S.

At both poles, time lapse imaging implies rotation in the same direction as the planet, i.e., cyclonic. Two of the three northern circumpolar cyclones have compact darker interiors, surrounded by brighter spiral-shaped clouds, with exteriors bounded by a narrow and dark periphery. In the south, three of the four southern circumpolar cyclones (Figure 2, labeled CPC), including the one closest to the south pole, lack the dark interior of their northern counterparts. They have a more extended dark periphery and are surrounded by a filigree-like pattern of lighter, spiral-shaped clouds. At lower latitudes, cyclones are rapidly changing and amorphous. Thus, Jupiter's polar atmosphere is not only dynamically unlike elsewhere at lower latitudes, but it is also unlike Saturn's polar atmosphere. For Saturn, many small anticyclones lie within the circumpolar jets. The small vortices close to Saturn's poles are located inside broad cyclonic features centered at the precise position of each pole [*Dyudina et al*., 2008; *Fletcher et al*., 2008; *Baines et al*., 2009; *Antuñano et al*., 2015], which we do not detect at Jupiter. This difference has been examined by *O'Neill et al*. [2015], who noted that cyclones naturally migrate to higher latitudes, but suspected that there might be no Saturn-like polar cyclones in Jupiter's atmosphere because of the absence of strong polar zonal jets compared with Saturn's higher vorticity gradient near its pole. Jupiter's relatively weak zonal jet structure within 30° of its poles is also consistent with the absence of any meandering feature, such as Saturn's hexagon, which is associated with a strong (100 m/s) jet.

4.3. Folded Filamentary Regions

Among the brightest and largest of discrete features in both poles are amorphously shaped regions for which we adapt the nomenclature of *Ingersoll et al*. [1979], "folded filamentary regions" (Figure 1, labeled "FFR"). These have been detected in the polar regions previously from Voyager, Cassini, and Hubble images [*Porco et al*., 2003; *Li et al*., 2004; *Barrado-Izagirre et al*., 2008], but not in such detail. They populate both polar regions right up to the circumpolar cyclones. The most compact of these regions, those less than 1000 km in size, are cyclonic. FFRs larger than this are chaotic and sprawling, with suggestions of rotation only in some substructures. In the north, the largest of these is roughly 4000 by 7000 km. There is an extended, chaotic region visible outside the high-latitude, dark-background part of the NPR between 54°N and 59°N, subtending some 80° in longitude in a region of weak retrograde winds [*Barrado-Izagirre et al*., 2008].

In the south, several FFRs are so concentrated between 68°S and 73°S latitude that they form a single feature that stretches over 70° in longitude (Figure 2, the lower feature labeled FFR). Another concentration forms a hook-like pattern between 72°S and 80°S stretching over 25° of longitude (Figure 2, the upper feature labeled FFR). The first of these is immediately poleward of the southern boundary of a strong (35 to 40 m/s) prograde jet centered at 69°S, in a region of weak (0 to 11 m/s) retrograde winds that stretches to 79°S [*Barrado-Izagirre et al*., 2008]. In the north, many FFRs are large enough to have been seen in the Cassini animation [*Porco et al*., 2003] moving irregularly past each other, with the largest features lasting throughout the entire 70 day period. Although Voyager and New Horizons imaging has identified high-latitude FFRs to be the source of lightning, particularly at 45°–49° with some at 53°–57°N [*Borucki and Magalhães*, 1992], so far no lightning has been identified in any of our images, including a long (52.1 ms) integration over the north pole in all color filters attempting to detect faint auroral emission. We note that similar features are apparent, although not as distinctly, in a Voyager-1 orange-filtered mosaic of the north pole with a correction for variations in illumination [*Rages et al*., 1999, Figure 3B]. Similar to the north, some chaotic regions are also present equatorward of the darkest part of the SPR, between 52°S and 63°S.

4.4. Ovals

Other features in both polar regions are primarily oval in shape. In the north polar region, they are all smaller than the FFRs (Figure 1, examples are labeled "Ovals") and lack readily discernable clues about their direction of rotation. The largest ovals are brighter than the background, but most are less reflective than the FFRs and even the CPCs. The biggest in the north is 1400 km across; smaller ones in the range of 200–700 km are dimmer. Much smaller ovals are barely brighter than the background clouds and range in size down to the JunoCam ~50 km spatial resolution.

In the south, the ovals are qualitatively different than those in the north, appearing as brighter versions of the southern CPCs. Several of the brightest and largest ovals lie near the longest extended FFR, between 71°S and

74°S, ranging in size from 200 km to 1000 km. There are large spiral extensions on these large ovals with a morphology that is consistent with anticyclonic rotation. Two ovals are visible closer to the pole near 80°S, both around 560 km in size, without any apparent spiral extensions. Unlike the CPCs, none appear to possess dark peripheral clouds. There are also some extremely small ovals between 53°S and 60°S, ranging in size from less than 2000 km down to the limit of JunoCam's resolution. These have extensive peripheral clouds that represent the darkest material we see in either the NPR or the SPR. Some of this same dark material is also found farther from the pole between latitudes 61°S and 66°S in the form of irregular "splotches" of approximately 1200–1600 km in size.

4.5. Linear Features

Our images show two narrow, elongated, "linear" cloud features in the NPR, denoted by a homogeneous interior that is lighter than the surrounding clouds and often bordered by a very narrow lane of darker material. One of these "streaks" begins in a relatively bland region near 66°N and extends through 30° of longitude, terminating at 62°N, widening from approximately 600 km to 1300 km between its eastern and western ends (Figure 1, labeled "L1"). The other begins at 68°N and is still visible 20°W of its eastern end right at the dawn terminator at 62°N, widening from approximately 1300 to 3100 km from its eastern end until it disappears past the dawn terminator (Figure 1, labeled "L2"). The latitude range of this feature appears to span a prograde jet peak at 65.6°N [*Porco et al*., 2003; *Barrado-Izagirre et al*., 2008] (see the insert in Figure 1). Thus, it is unlikely to be associated with the tropospheric clouds used to track wind speeds in these studies, unless its lifetime, or at the very least its morphology as observed during PJ1, is relatively short. It is more likely that it and probably feature L1 are associated with a high-altitude stratospheric haze. The L2 feature is close to a similar feature in an associated methane image (Figure S1 in the supporting information), implying that it is related to a high-altitude haze (a similar region for the L1 feature lies in a saturated region of the methane image). *Barrado-Izagirre et al*. [2008] specifically identify this latitude with a wave structure that is most apparent in similar Hubble Space Telescope and Cassini Imaging Sub-System methane filters. They place this haze at and above the 100 mbar level. No similar features are detectable in the SPR, where only a few very short straight, dark lines are visible, despite the prominence of a polar haze boundary in our methane-filter image (supporting information Figure S2).

4.6. High-Altitude Cloud

A high-altitude cloud feature was detected well into the nighttime side of the dusk terminator (Figure 1, labeled "HAC"), located at 63°N latitude and 70°W longitude. It is evident not only in this image but also in two subsequent images, 6162 and 6163, taken shortly after 6160, at 11:59 and just before 12:02 UT, respectively. The feature appears without enhancement most clearly in 6163, the long-exposure RGB image described earlier that was designed to detect auroral features on Jupiter's nightside (none were detected). Figure 3a shows an excerpt of a cylindrical projection of this image centered on this feature. A fully illuminated version of the same region is shown in Figure 3b, taken from a lower resolution image in the last of the inbound marble movie images, before the close-up images that began with Figure 1. Only part of the southern half of the feature is recognizable, implying that it is optically thin. A similarly illuminated version of the same region imaged by the JunoCam methane filter at 890 nm is shown in Figure 3c. This image is more sensitive to particles closer to the upper tropopause near ~200 mbar and lower atmospheric pressures. This panel appears more "blocky" as a result of the strong compression that was being tested during PJ1 for this wavelength. Nonetheless, it illustrates a key point, if we assume that the somewhat brighter region to the east of ~69°W longitude in the "methane" image (Figure 3c) represents the same high-altitude feature as shown in Figure 3a. The fully illuminated feature extends farther eastward in the methane image (Figure 3c), out to 63°W, than the color composite at the terminator (Figure 3a) where it only reaches 66–67°W. This implies that the apparent eastern edge in Figure 3a is purely the result of illumination geometry, as illustrated schematically in Figure 3d.

Figure 3d shows the relationship between distance from the terminator and altitude. Because the HAC is likely to be optically thin, it might also be a physically thin layer, as shown, as opposed to a towering cloud whose base is in shadow. Using the simple geometric relationship shown in the figure, we can determine the altitude of this cloud above the "main" cloud deck. Figure 3e shows our attempt to provide a measurement of the angular distance θ, using the distance from the terminator provided by the geometric calibration of the image and (a) the peak radiance of the feature, after subtracting the background outside the feature, as

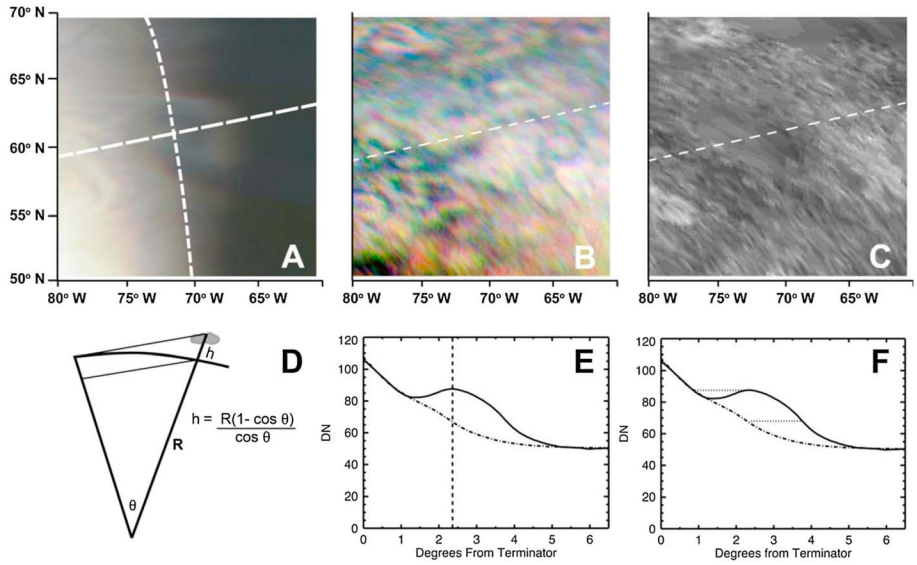

Figure 3. Nighttime-illuminated high-altitude cloud (labeled HAC in Figure 1). (a) An excerpt from a cylindrical-map projection of JunoCam image in linear (longitude, latitude) coordinates showing the feature. This image, number 6163, was taken on 27 August 2016, just before 12:02 UT. The location of the terminator from geometric calibration is illustrated by the short-dashed curve and the direction of sunlight in the center of the feature by the long-dashed line. A System-III longitude scale and a planetocentric latitude scale are provided for reference. (b) The same feature in an earlier exposure on the dayside of Jupiter from an image taken on the same day at 10:46 UT, image 6159. A lighter version of the long-dashed line in Figure 3a is repeated in this panel and Figure 3c. (c) The feature in daylight in JunoCam's methane filter at 10:30 UT, image 6158. (d) The geometric relationships that allow us to determine the altitude of a high-cloud feature from its angular distance from the terminator. The tall cloud in the illustration could also be a thin cloud illuminated above the nightside of Jupiter at the same altitude as the peak of this cloud or a laterally extended cloud rather than a discrete one. (e) The radiance in raw data numbers ("DN") along a cut along the dashed line in Figure 3a as a function of angular distance from the terminator (dotted line in Figure 3a). The alternating dash-dotted lines show the same cut but through a broad stretch of latitudes to the north and to the south of the feature in Figure 3a. The vertical dashed line shows the location of the peak radiance. (f) An alternative method of measuring the distance between the terminator and the high-altitude cloud by measuring the distance between equivalent radiances at the terminator and those at the nighttime edge of the feature.

shown by the dotted line, or (b) the half power of the feature farthest from the terminator. However, differences between the assigned location of the terminator in images 6160, 6162, and 6163 at this time were far in excess of the small differences expected in the ~3 min separating their acquisition times, yielding uncertainties in the determination of the altitude in excess of 50% of the derived value. Instead, we took an empirical approach, illustrated in Figure 3f: estimating θ by taking the distance between equal radiances at the terminator and at the eastern edge of the feature. We avoided a systematic offset due to higher radiances within the feature itself by using radiances outside the feature up to 13° away in latitude both north and south along lines parallel to the geometrically defined terminator (dashed line in Figure 3a). Using this approach, we derived a value of 58 ± 21 km for the height of this feature above the average background cloud layer. We use the standard deviation to represent the uncertainty, rather than the error of the mean (a factor of 3 smaller for measurements made by three filters in three images), because this value represents not only the divergence of results from the three images but also the spread between the three filters, with the blue-filter value always smaller than those derived from the red- and green-filtered images. The reason for this difference is not understood.

The only previous phenomena similar to the HAC are the shadows that were detected in mesoscale waves near the terminator in New Horizons observations [*Simon et al*., 2015], but these were at much lower latitudes. *Rages et al*. [1999] detected polar haze layers near the same high latitude using Galileo high-resolution images of Jupiter's limb. Their haze layer was detected at only one location, not dissimilar to our detection at only a single location and in one polar region. Their model-dependent derived vertical positions of the responsible haze layer range from 1.1 to 27 mbar or physical altitudes from 40 to 135 km above the 1 bar level. This is not far from an expected location of ammonia gas saturation, which would be at ~700 mbar

for the ~3 times solar NH_3 abundance measured by the Juno Microwave Radiometer experiment in the deep troposphere [*Bolton et al*., 2017], taking protosolar $N/H = 7.41 \times 10^{-5}$ [*Asplund et al*., 2009]. However, NH_3 is found to be depleted in the upper troposphere by Juno and previously by the Galileo probe, which would raise the saturated level to lower atmospheric pressures [*Atreya et al*., 1999; *de Pater et al*., 2001]. The HAC does not appear to be correlated with any clouds resulting from strong upwelling of NH_3, NH_4SH, or H_2O gas or their condensates [*Atreya et al*., 1999], especially considering that the HAC is not a towering cloud or optically very thick. One possibility is that the HAC is directly related to local auroral processes, similar to the "south dark patch" reported previously within the south auroral oval [*Vincent et al*., 2000; *Porco et al*., 2003]. We believe this is unlikely because the feature is physically distant from the auroral oval, which is centered closer to 180°W longitude [*Bonfond et al*., 2012, 2017; *Connerney et al*., 2017; *Dinelli et al*., 2017], illustrated in Figures S1 and S3 in the supporting information. Alternatively, the HAC could be related to the haze of complex hydrocarbons expected to form in the stratosphere [*Atreya et al*., 2005], either directly or indirectly by the hydrocarbon haze particles facilitating the formation of a thin ammonia cloud/haze layer in the lower stratosphere. The hydrocarbon chemistry at auroral latitudes of the HAC is governed by the precipitation of magnetospheric charged particles that can, in fact, be nonuniform. Earlier measurements of the haze [e.g., *Vincent et al*., 2000; *Porco et al*., 2003; *Barrado-Izagirre et al*., 2008] illustrate its nonuniformity, which is clearly influenced by both auroral-related chemistry and stratospheric transport, neither of which is well characterized quantitatively yet. Further elucidation of the correspondence between JunoCam results, the Galileo haze layer, and models of atmospheric chemistry and dynamics in polar regions will be enabled by the additional constraints provided by the 5 μm imaging and 2–5 μm spectroscopy supplied by observations of the same region by Juno's JIRAM instrument, providing additional constraints on cloud and haze layer altitudes.

5. Conclusions

JunoCam imaged Jupiter's polar regions at visible wavelengths with 50 to 70 km spatial scales for the first time. These images confirmed a breakdown of the predominantly east-west structure poleward of 68°N latitude and 64°S latitude, immediately poleward of ~40 m/s prograde jets. Circumpolar cyclones were detected within 6° of each pole with roughly regular longitudinal spacing, but no Saturn-like polar cyclones were detected, confirming the prediction of *O'Neill et al*. [2015]. Ovals were detected farther from the poles. Ovals in the NPR and SPR had subtle morphological differences. The largest regions, rather complicated and chaotic in shape, were labeled folded filamentary regions after short-lived counterparts at lower latitudes. These are likely to be regions lasting throughout 70 days of monitoring by the Cassini imaging experiment. A high-altitude feature was detected past the nominal location of the terminator at one location in the NPR, which is likely to be optically thin. This feature could correspond to high-altitude hazes 40–137 km above the 1 bar level detected at some locations in the NPR by the Galileo mission. It could be the product of a localized updraft of saturated air, resulting in a thin condensate layer, or, alternatively, it could be directly or indirectly related to a nonuniform distribution of auroral-related hydrocarbon haze particles.

JunoCam will acquire polar images on every perijove. These images will allow us to track, at 53 day intervals, the state and evolution of the polar clouds and storms. As the petal of Juno's elliptical orbit rotates into the southern hemisphere the perijove moves to more northerly latitudes, decreasing the altitude of the spacecraft over the NPR at low emission angles, allowing higher-resolution images. Additional insight will also be gained by combining results from JunoCam and other Juno instruments, together with supporting Earth-based synoptic observations.

Acknowledgments
This research was funded by the National Aeronautics and Space Administration through the Juno Project. A portion of these funds were distributed to the Jet Propulsion Laboratory, California Institute of Technology. All JunoCam images can be obtained on the Mission Juno web site (https://www.missionjuno.swri.edu), via its links to the JunoCam instrument, then to "Processing." We acknowledge invaluable help from John Rogers, Gerald Eichstädt, Leigh Fletcher, Brendan Fisher, and two anonymous reviewers. We thank Liming Li and Naiara Barrado-Izagirre for digital versions of the wind speed profiles shown in Figures 1 and 2.

References

Antuñano, A., T. Río-Gazelurrutia, A. Sánchez-Lavega, and R. Hueso (2015), Dynamics of Saturn's polar regions, *J. Geophys. Res. Planets*, *129*, 155–176, doi:10.1002/2014JE004709.

Asplund, M., N. Grevesse, J. Sauval, and P. Scott (2009), The chemical composition of the Sun, *Ann. Rev. Astron. Astrophys.*, *47*, 481–522.

Atreya, S. K., M. H. Wong, T. C. Owen, P. R. Mahaffyc, H. B. Niemannc, I. de Paterd, P. Drossarte, and T. Encrenaz (1999), Comparison of the atmospheres of Jupiter and Saturn: Deep atmospheric composition, cloud structure, vertical mixing, and origin, *Planet. Space Sci.*, *47*, 1243–1262.

Atreya, S. K., A. S. Wong, K. H. Baines, M. H. Wong, and T. C. Owen (2005), Jupiter's ammonia clouds—Localized or ubiquitous, *Planet. Space Sci.*, *53*, 498–507.

Baines, K. H., T. W. Momary, L. N. Fletcher, A. P. Showman, M. Roos-Serote, R. H. Brown, J. B. Buratti, R. N. Clark, and P. D. Nicholson (2009), Saturn's north polar cyclone and hexagon at depth revealed by Cassini/VIMS, *Planet. Space Sci.*, *57*, 1671–1681.

Barrado-Izagirre, N., A. Sánchez-Lavega, S. Pérez-Hoyos, and R. Hueso (2008), Jupiter's polar clouds and waves from Cassini and HST images: 1993–2006, *Icarus*, *194*, 173–185.

Bolton, S. J., J. E. P. Connerney, S. M. Levin, and the Juno Science Team (2017), Jupiter's interior and deep atmosphere: The initial pole-to-pole passes with the Juno spacecraft, *Science*, doi: 10.1126/science.aal2108, in press.

Bonfond, B., D. Grodent, J.-C. Gerard, T. Stallard, J. T. Clarke, M. Yoneda, A. Radioti, and J. Gustin (2012), Auroral evidence of Io's control over the magnetosphere of Jupiter, *Geophys. Res. Lett.*, *39*, L01105, doi:10.1029/2011GL050253.

Bonfond, B., et al. (2017), Morphology of the UV aurorae Jupiter during Juno's first perijove observations, *Geophys. Res. Lett.*, doi:10.1002/2017GL073114, in press.

Borucki, W. J., and J. A. Magalhães (1992), Analysis of Voyager 2 images of Jovian lightning, *Icarus*, *96*, 1–14.

Connerney, J. E. P., et al. (2017), Jupiter's magnetosphere and aurorae observed by the Juno spacecraft during its first polar orbits, *Science*, doi: 10.1126/science.aam5928, in press.

de Pater, I., D. Dunn, P. Romani, and K. Zahnle (2001), Reconciling Galileo Probe data and ground-based radio observations of ammonia on Jupiter, *Icarus*, *149*, 66–78.

Dinelli, B. M., et al. (2017), Preliminary Jiram results from Juno polar observations: 1. Methodology and analysis applied to the Jovian northern polar region, *Geophys. Res. Lett.*, doi:10.1002/2017GL072929, in press.

Dyudina, U. A., et al. (2008), Dynamics of Saturn's south polar vortex, *Science*, *319*, 1081.

Fletcher, L. N., et al. (2008), Saturn's polar dynamics: Temperature and composition of the hotspots and hexagon, *Science*, *319*, 79–81.

Gehrels, T. (1976), Results of the Imaging Photopolarimeter on Pioneers 10 and 11, in *Jupiter: Studies of the Interior, Atmosphere, Magnetosphere and Satellites*, edited by T. Gehrels, pp. 531–563, Univ. Arizona Press, Tucson.

Godfrey, D. A. (1988), A hexagonal feature around Saturn's north pole, *Icarus*, *76*, 335–356.

Hansen, C. J., M. A. Caplinger, A. Ingersoll, M. A. Ravine, E. Jensen, S. Bolton, and G. Orton (2014), JunoCam: Juno's outreach camera, *Space Sci. Rev.*, doi:10.1007/s/11214-014-0079-x.

Ingersoll, A. P., R. E. Beebe, S. A. Collins, J. L. Mitchell, R. J. Terrile, G. E. Hunt, P. Muller, and B. A. Smith (1979), Zonal velocity and texture in the Jovian atmosphere inferred from Voyager images, *Nature*, *280*, 773–775.

Li, L., A. P. Ingersoll, A. R. Vasavada, C. C. Porco, A. D. Del Genio, and S. P. Ewald (2004), Life cycles of spots on Jupiter from Cassini images, *Icarus*, *172*, 9–23.

O'Neill, M., K. E. Emanuel, and G. R. Flierl (2015), Polar vortex formation in giant-planet atmospheres due to moist convection, *Nat. Geosci.*, *8*, 523–526.

Porco, C., et al. (2003), Cassini imaging of Jupiter's atmosphere, satellites, and rings, *Science*, *299*, 1541–1547.

Rages, K., R. Beebe, and D. Senske (1999), Jovian stratospheric hazes: The high phase angle view from Galileo, *Icarus*, *139*, 211–236.

Rogers, J. (1995), *The Giant Planet Jupiter*, 418 pp., Cambridge Univ. Press, Cambridge, U. K.

Simon, A. A., L. Li, and D. C. Reuter (2015), Small-scale waves on Jupiter: A reanalysis of New Horizons, Voyager, and Galileo data, *Geophys. Res. Lett.*, *42*, 2612–2618, doi:10.1002/2015GL063433.

Vincent, M. B., et al. (2000), Jupiter's polar regions in the ultraviolet as imaged by HST/WFPC2: Auroral-aligned features and zonal motions, *Icarus*, *143*, 205–222.